Overall evaluation:

The manuscript proposed a land surface image assimilation system capable of optimizing the spatial structure of the background field, and the ERA5-Land soil moisture reanalysis data was used as ideal observation to validate the assimilation system. The results of ideal experiments showed that the proposed image assimilation system exhibits a remarkable ability to adjust the spatial structure of soil moisture in a land surface model, considerably improving the prediction skill. This is an interesting study. However, the manuscript is not written well and lacks in-depth analysis. For example, in the section "Discussion and conclusions", it would be useful to add more information comparing the proposed assimilation system with existing assimilation systems.

Response:

Thanks to your valuable comments and suggestions. Following your suggestions, we have made more deep analysis and revised the manuscript carefully from the beginning to the end.

(1) The conclusion and discussion part has been further refined, encompassing a recapitulation of significant findings for the study, and an emphasis on the limitations and future prospects of image assimilation methods, as well as the inclusion of comparative analysis with existing studies. The revised version of the conclusion in Line 662-705 is presented below:

The exchange of heat and water vapor between the land surface and the atmosphere plays a crucial role in influencing weather and climate change. The impact of soil moisture on atmospheric changes is frequently manifested through the persistent influence of large-scale soil moisture anomalies. The construction of an assimilation system with image assimilation capability is aimed at enhancing the spatial structure accuracy of soil moisture anomalies in the initial field of land surface models. The system is primarily based on the three-dimensional variational data assimilation framework, employing the curvelet transformation method with multi-scale transformation capability and anisotropic basis function as the observation operator. By incorporating image structural similarity as a weak constraint in the cost function, the spatial structure of soil moisture in the initial condition is effectively adjusted to align with the structural characteristics of observed soil moisture image, thereby enhancing the accuracy of soil moisture simulation.

The performance of the image assimilation system is systematically validated by conducting ideal experiments, with the ERA5-Land reanalysis data as ideal observations, and the CLDAS reanalysis product is incorporated for independent verification. The findings demonstrate that the assimilation of surface soil moisture observation images effectively and reasonably enhances the spatial structure of soil moisture analysis field. The spatial correlation coefficient between the analysis and ERA-Land reanalysis data increases significantly from 0.39 to 0.67, while the root-mean-square error decreases notably from 0.16 m^3/m^3 to 0.12 m^3/m^3. With the improvement of surface soil moisture, the spatial pattern of subsurface soil moisture is further optimized under the reasonable constraints of model dynamics and thermal processes. There is an increase (from 0.35 to 0.57) in the spatial correlation coefficient between the soil moisture at a depth of 7–28 cm and the ERA-Land data. The root mean square error decreases from 0.15 m^3/m^3 to 0.13 m^3/m^3.

The verification results based on independent data CLDAS consistently demonstrate a higher spatial correlation coefficient between CoLM surface (0–5 cm) soil moisture in the assimilation experiment and the CTL experiment, with a maximum correlation coefficient of 0.79 throughout both assimilation and prediction stages. The average spatial correlation coefficient for surface soil moisture increases from 0.67 to 0.71 after image assimilation. While for subsurface (5–10 cm) soil moisture, it steadily rises from 0.67 to 0.73 on average. These quantitative evaluation outcomes fully validate the practical applicability of the new image assimilation method.

The image assimilation system developed by this study could effectively optimize the spatial structure of soil variables in the background by incorporating constraint conditions of the observed spatial structures. The method demonstrates excellent applicability to various soil variables, effectively mitigating the negative impact of strong spatial heterogeneity of soil on data assimilation. The key challenge in image assimilation lies in obtaining accurate spatial structure observation of soil variables. The data of ground automatic stations with high spatial-temporal resolution established in China, along with satellite observation data that can overcome natural constraints and achieve large-scale uniform observation in various terrains, are capable of providing observational images depicting the spatial structure of land surface variables for image assimilation. The effective assimilation of the spatial structural characteristics of those high-density meteorological observation data, is the primary focus of our subsequent research. However, how to establish the direct spatial structure relationship between

satellite-observed brightness temperature data and soil variables, and how to repair these non-uniform data into uniformly distributed data, these are the key technical problems that need to be solved in the future.

Additionally, it should be noted that the image assimilation method and the prevailing single-point land assimilation method in current practice are not mutually exclusive. The single-point land assimilation method is more suitable for assimilating sparse observation data in key areas. However, if the image assimilation method is used to optimize the fine structure of soil moisture in specific areas, the threshold σ mentioned above needs to be further increased, but this approach is susceptible to introducing additional observational errors. Therefore, by integrating the capacity of the image assimilation method in adjusting the large-scale spatial structure of soil variables and the capability of single-point land assimilation method in finely optimizing soil variables in crucial regions, and by leveraging the advantages offered by diverse types of meteorological observation data, we can attain more refined initial conditions for land models, which constitutes the primary objective of our subsequent research.

(2) In addition, the following experiments and analysis for choosing the threshold of 0.5 for the curvelet denoising have been incorporated to enhance the depth of analysis in the manuscript.

The image assimilation system determines the spatial structural characteristics of assimilation according to the threshold values, and different threshold values could result in certain variations in the spatial structure of assimilation. Naturally, a higher threshold can capture more spatial structural features of the observed variables, but the presence of observation errors imposes limitations on its continuous increase. More discussions have been added to the revised manuscript in Line 366-404 to prove that a threshold of 0.5 can not only capture the spatial structure information of observation data, but also mitigate the impact of observational errors. The specific content comprises the following three aspects:

A. The definition of the threshold σ has been further elaborated in order to provide a clearer rationale for its selection. This detailed description has been incorporated into line 370-371 of the revised manuscript. The specific wording is as follows:

The threshold σ means the modulus of the decomposition coefficient falls within the first 100*σ%

85 percentile. For instance, a value of 0.5 indicates that the mode retaining the top 50% of decomposition coefficient.

B. By employing the spatial correlation method, we demonstrate that a threshold of 0.5 adequately captures the primary spatial information derived from soil moisture observations, the following discussions have been added to Line 366-404 of the revised manuscript:

90 The image assimilation system finds the spatial structural characteristics of assimilation according to the threshold values, and different thresholds could result in certain variations in assimilated spatial structure. In order to clarify the spatial structure differences corresponding to different thresholds, the spatial correlation method (Daley, 1991) is employed in this study to elucidate the distinctive characteristics of spatial structure corresponding to varying thresholds.

95 The hourly soil moisture data from ERA5-Land from May 1 to 30, 2016 is selected for analysis. The threshold σ means the modulus of the decomposition coefficient falls within the first 100*σ% percentile. For instance, a value of 0.5 indicates that the mode retaining the top 50% of decomposition coefficient. The original image can be reconstructed by selecting different threshold ranges, namely (0,0.01], (0.01,0.03], (0.03,0.05], (0.05,0.1], (0.1,0.2], (0.2,0.3], (0.3,0.4], (0.4,0.5], (0.5,0.6], (0.6,0.7],

100 (0.7,0.8], (0.8,0.9] and (0.9,1.0]. The correlation coefficient between each grid point and its neighboring grid points can be obtained based on the reconstructed time series of each grid point. The spatial structural characteristics of different scales in the reconstructed images could be quantitatively expressed by the average correlation coefficients corresponding to different grid point distances.

The mean correlation coefficient corresponding to grid point distance is illustrated in Figure 4. As

105 can be seen, the variation characteristics of the inter-grid correlation coefficient of the original soil moisture represented by the black line with respect to the grid distance. The average correlation coefficient can exceed 0.5 within a radius of 200 km, while maintaining above 0.4 within a radius of 300 km. The distance corresponding to high correlation coefficients represents the characteristics of consistent changes in soil moisture within a similar range, that is, soil moisture has the characteristics

110 of spatial structure at the corresponding scale.

When the threshold value is 0.01, the average correlation curve exhibits a similar change in correlation coefficient of the original variable, thereby indicating that the curvelet coefficient corresponding to this threshold value effectively reproduces the large-scale spatial structure. The

spatial structure scale represented by the corresponding curvelet transformation reconstruction results decrease as the threshold value increases, leading to a rapid decrease in the correlation coefficient with increasing distance. The curvelet reconstruction results with different threshold intervals represent the structural characteristics of different horizontal scales, while the cumulative threshold can well represent the spatial structural characteristics of soil moisture variables represented by the selected threshold in the assimilation. The average correlation coefficient of the cumulative threshold is depicted in Figure 4b. As can be seen, the top 10% of curvelet coefficients can effectively replicate the spatial correlation characteristics of soil moisture variables. The results also indicate that the variations in threshold values have minimal impact on the assimilated spatial structure when the threshold value exceeds 0.1.

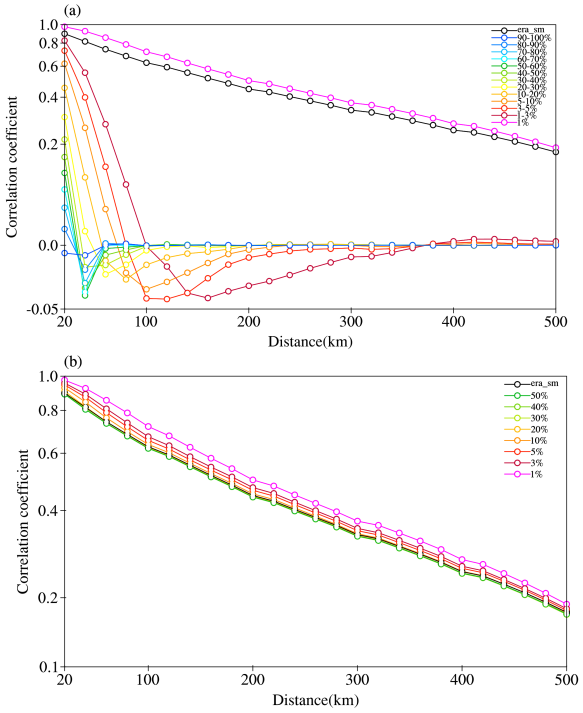

Figure 4: Variation curves of the average correlation coefficient between grid points with the distance in the reconstructed ERA5-Land hourly soil moisture image of the study area from May 1 to 30, 2016, which is reconstructed based on the curvelet coefficients of (a) different threshold intervals and (b) cumulative thresholds.

C. According to the stochastic characteristics of observation errors, we conducted an analysis on the probability distribution properties of the reconstructed residuals and found that a threshold value of 0.5 effectively mitigates the impact of observation errors.

Naturally, a higher threshold can effectively capture more spatial structural features of the observed variables, but the presence of observation errors imposes limitations on its continuous increase. The observational error is typically characterized by stochastic fluctuations. When the discrepancy between the reconstructed results and the original variables exhibits random variation characteristics, it can be inferred that the observation information eliminated by the threshold method primarily consists of observation errors.

To better clarify the statistical characteristics of the reconstruction errors under different thresholds, Figure 5 shows the probability density distribution curves of the reconstruction errors for 100 reconstructed fields at different thresholds. For the error at the threshold of 0.5, the skewness coefficient of the probability density distribution curve is 0.00 and the kurtosis coefficient is 0.38, indicating the curve is close to the standard normal distribution curve (the skewness and kurtosis coefficients are all 0). With the gradual increase of threshold value, although the reconstruction error decreases, the residual error is mainly concentrated in the range of smaller values, and the curve shows a "sharp peak" distribution. Considering that the observation errors are mostly random errors, it is reasonable to believe that the reconstruction errors at the threshold of 0.5 are mainly observation errors, which also implies this threshold is good for the purpose of denoising the observation images.

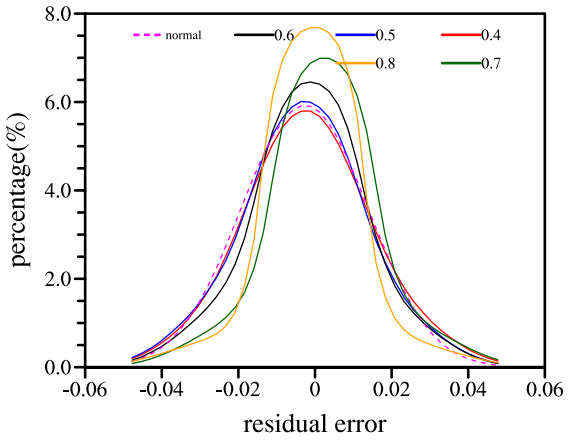

Figure 5 Probability density distributions of 100 reconstructed errors under different thresholds. The magenta dashed line represents standard normal distribution. The red, blue, black, green and orange solid lines represent threshold values of 0.4, 0.5, 0.6, 0.7 and 0.8, respectively.

The revised manuscript now includes the newly added Figure 4, which has been incorporated into the section on observational error analysis along with its corresponding discussion.

And the relevant reference has been added to the revised manuscript:

Daley, R.: Atmospheric Data Analysis, Cambridge University Press, Cambridge, 1991.

(3) We have added a specialized section in the revised manuscript to facilitate a comparative analysis of the disparity in the effectiveness between the prevailing single point assimilation method and image assimilation method.

3.4 The influence of image assimilation constraints

Two sets of ideal experiments are designed to validate the impact of image assimilation and evaluate its superiority over traditional single column assimilation in adjusting the spatial distribution structure of soil moisture. The ideal observational data for assimilation is the ERA5-Land reanalysis soil moisture. The first set corresponds to the conventional assimilation experiment, where $J_{(x)} = J_B + J_o$, as described by Equation (5). Another set is image assimilation experiment, where $J_o = 0$ in Equation (5), indicating that $J_{(x)} = J_B + J_I$.

The process of data assimilation entails leveraging the discrepancy between observed data and background field, in conjunction with a priori knowledge of observation error and background error, to derive an analysis field that closely approximates the true value. The primary challenge in single column assimilation lies in acquiring precise prior information regarding observation error. The spatial distribution of observation error for a specific single column assimilation experiment is illustrated in Fig. 6. In consideration of the necessity for an ideal experiment, it is assumed that the observation error outside the China region is negligible, while a significant error is presumed within the China region, so as to emphasize the impact of observation error on assimilation results.

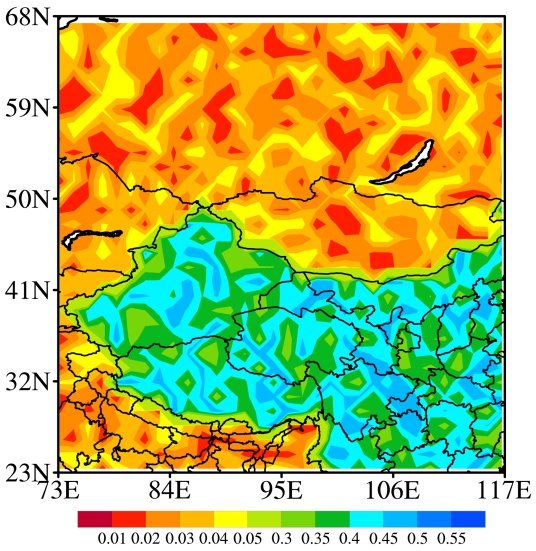

Figure 6: Spatial distribution of observation errors.

The spatial distributions of soil moisture for the ideal observation data and different experiments at 0000 UTC on May 1, 2016 are given in Figure 7. The spatial distribution of surface soil moisture in ERA5-Land is illustrated in Fig. 7a. The northern Siberian region of the selected area exhibits a relatively high soil moisture content overall, with a ring-shaped distinct wet zone in the northwest. The central region stretching from Xinjiang to western Mongolia is a significant arid area. However, the soil moisture in the Tianshan Mountains is wet. The soil moisture of the Qinghai-Tibet Plateau region gradually decreases from west to east. The soil moisture in southern Qinghai, Hunan and Jiangxi is characterized by high level of saturation, while Gansu, Ningxia and Hebei experience relatively arid soil conditions. Figure 7b is the distribution of soil moisture in the control experiment (background field). It is evident that there are significant disparities in the spatial distribution of soil moisture when compared with the reanalysis data. In the control experiment, a dry region extends from west to east in the northern area of Lake Baikal, while eastern Kazakhstan and central Inner Mongolia also exhibit arid conditions.

Figure 7c shows the results of the single point assimilation experiment. The observation error outside the China region is relatively minimal, indicating a strong correspondence between the analysis field and the observation data, and the overall distribution also exhibits a high degree of conformity with the observation. The analysis field in China region, however, closely resembles the background field. Nevertheless, there is a significant disparity between the observed soil moisture and that of the background field, indicating a lack of adjustment based on observed information.

Figure 7d is the assimilation results of the image assimilation ideal experiment. It is evident that image assimilation effectively adjusts the distribution pattern of soil moisture. The above-mentioned characteristics of moist soil moisture in the northwest region of the observation field, the arid region of Xinjiang and Mongolia, and the humid region of the Tianshan Mountains are all well reflected in the analysis field.

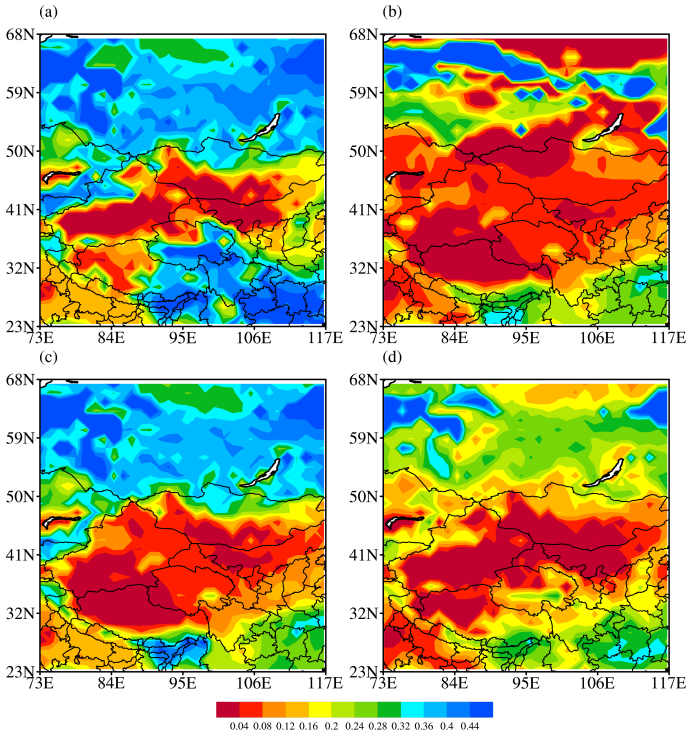

Figure 7: Spatial distributions of surface soil moisture for (a) ERA5-Land, (b) CTL experiment, (c) analysis field of conventional assimilation experiment, and (d) analysis field of image assimilation experiment at 00:00 UTC on May 1, 2016.

The analysis results mentioned above have been added into the revised manuscript. Please refer to Line 236 for detailed information.

(4) We attempted to explain the underlying physical mechanisms how the surface soil moisture assimilation improves deep soil moisture, which are elucidated through a vertical-time profile of soil moisture. The following additional figures and associated descriptions have been added to lines 155-158 of the revised manuscript:

Soil moisture and its vertical transport is governed by infiltration, runoff, gradient diffusion, gravity, and root extraction by canopy transpiration. Only the vertical transport of soil water is considered in the CoLM model. The water in the soil will percolate through the soil pores due to the combined effects of gravity and capillary forces. According to the principle of mass conservation, the vertical movement of soil water can be mathematically described by the Richards equation.

$$\frac{\partial \theta}{\partial t} = -\frac{\partial q}{\partial z} - E - R_{fm}$$

And the relevant description has been added to the revised manuscript in Line 524-531:

Vertical motion of soil water is integrated over the layer thickness, in which the time rate of variation in water mass must equal to the net flow across the bounding interface, and plus the rate of internal source or sink. The terms of water flow across the layer interfaces are linearly expanded by using first-order Taylor expansion. Therefore, when the surface data were assimilated, the net flow across the bounding interface to deeper layers become more reasonable corresponding to surface variation.

Of course, when it comes to the process of permafrost and snow processes, such as soil freezing and thawing in the Tibetan Plateau region, the variations of soil moisture are much more complex, and the mechanism of data assimilation on permafrost needs to be studied more thoroughly in the future.

In addition, the subsequent soil moisture time-depth profiles of real experiments are utilized to elucidate the process by which surface soil moisture assimilation impacts deep soil moisture. The following figure and related discussions are added to Line 532-573 of the revised manuscript:

In order to further elucidate the vertical impact of data assimilation, the vertical propagation characteristics of surface assimilation influence are also examined based on actual experiment results. The vertical-temporal profiles of soil moisture on different underlying surface types selected in the Tibetan Plateau and plain areas are given in Fig. 12, so as to elucidate the physical processes how the surface soil moisture assimilation influences soil moisture at a depth of 7–28 cm. The spatial locations of selected single points are depicted in Fig. 12a. In order to emphasize the soil moisture variation difference between plateau areas and plain areas, bare soil points are situated in the eastern and western regions of the plateau (represented by blue and black five-pointed stars), while corn and needleleaf evergreen boreal tree (represented by red and orange five-pointed stars) are positioned within the plain area. Figs. 12b–12c illustrate the difference of soil-moisture analysis field between DA experiment and CTL experiment, as well as the temporal characteristics of soil moisture analysis field at different depths of selected points in plateau areas. The vertical ordinate denotes the position of node depth for each soil layer in the CoLM model. The most notable difference in the vertical variation of soil moisture among the two points on the plateau is primarily attributed to the differences in both magnitude and depth of this vertical change. In the western plateau region, soil moisture at bare soil points is generally low, usually below 0.2 m3/m3 (Fig. 12b). Additionally, the surface undergoes significant temporal variations that may be related to the prevalence of small-scale convective weather

systems in this plateau area. The vertical variation of bare soil moisture in the plateau region primarily occurs above 50 cm, while the soil moisture exhibits a consistent pattern below 50 cm. The vertical variation of soil moisture is correlated with the intensity of soil moisture anomaly. As depicted in Figs. 12b and 12c, the vertical impact of minor perturbations in bare soil moisture within the plateau region is negligible, primarily occurring above a depth of 3 cm. The similarity between the two bare soil points lies in the fact that significant changes in soil moisture can rapidly impact the top 10 cm of soil, resulting in similar characteristics observed in the soil moisture above this depth. However, abnormal soil moisture exhibits a noticeable time lag effect below 10 cm. The characteristics of assimilation influence exhibit similarities to the features observed in vertical changes of soil moisture. Assimilation significantly enhances surface soil moisture around July 10th, and the increasement in soil moisture analysis within the plateau region can also rapidly impact the 10 cm depth of soil, with a maximum positive analysis increment reaching 0.16 m3/m3. The impact of assimilation can affect soil moisture at a depth of approximately 10 cm within one day, while it takes approximately 15 days for this analysis to affect the 50 cm depth. However, the impact of the analysis increment can be sustained for over a month at the depths ranging from 20 cm to 50 cm.

Figures 12d and 12e are similar to Figs. 12b and 12c, but they are selected from the plain areas. It is evident that the vertical variation characteristics of soil moisture differ significantly among different vegetation types. The analysis increment for corn is relatively minimal. Image assimilation leads to a substantial increase in surface soil moisture around July 10th. The maximum positive analysis increment can reach up to 0.12 m3/m3, with a vertical change level reaching approximately 30 cm. The effect is gradually transmitted to a depth of approximately 2 meters over time, with a duration of about one month. In the case of needleleaf evergreen boreal tree, the analysis increment is relatively small, and surface soil moisture gradually increases from around July, with its influence extending to a depth of approximately 100 cm. Seen from the above analysis, it is evident that the assimilation of surface soil moisture gradually impacts the deeper layers of the model as integration progresses, with a lasting effect of approximately 1 month. This phenomenon also serves as the primary factor contributing to the simulation improvement of soil moisture at a depth of 7–28 cm.

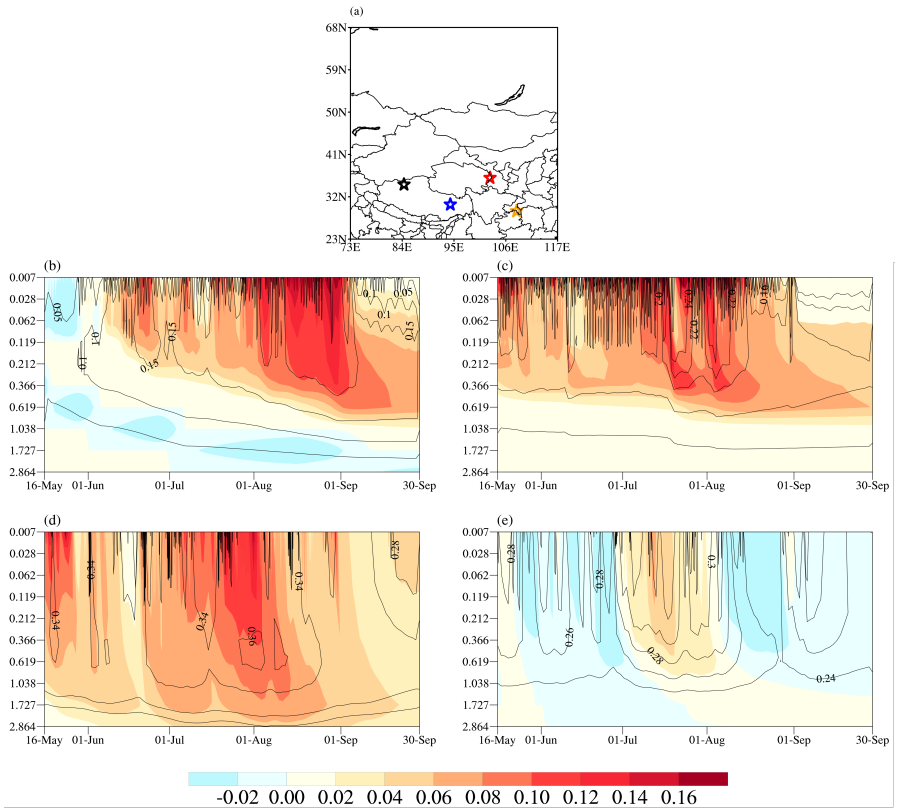

Figure 12: (a) The location of designated grid. The soil-moisture temporal variation of the difference between the DA experiment and CTL experiment (represented by shadow) and the soil moisture profiles (indicated by contours) under different land types: (b) bare soil (black five-pointed star), (c) bare soil (blue five-pointed star), (d) corn (red five-pointed star), and (e) needleleaf evergreen boreal tree (orange dots).

And the point-by-point response is listed below according to your specific comments.

Minor comments:

Line 18: Please use the official name: ERA5-Land.

Response:

Thank you for your valuable suggestion. We have revised the word “ERA5_Land” to “ERA5-Land” throughout the manuscript

Line 113: "five snow layers" -> "a maximum of five snow layers".

Response：

Thank you for your valuable suggestion. We have revised the words "five snow layers" in Line 154 to "a maximum of five snow layers".

Line 125: Please add reference to the atmospheric forcing data.

Response:

Thank you for your valuable suggestion. We have added the reference and relevant information about the forcing data in Line 170-176 as follows.

The forcing dataset was derived through combining observation-based analyses of monthly precipitation and surface air temperature with intramonthly variations from the National Centers for Environmental Prediction-National Center for Atmospheric Research (NCEP-NCAR) reanalysis. To correct the spurious long-term changes and biases in the NCEP-NCAR reanalysis precipitation, surface air temperature, and solar radiation fields, Qian et al. (2006) combined the intramonthly variations from the NCEP-NCAR 6 hourly reanalysis with monthly time series derived from station records of temperature and precipitation. It is shown that the CLM3 reproduces many aspects of the long-term mean, annual cycle, interannual and decadal variations when it was forced by this dataset.

The reference which has been added to the revised paper is as follows :

Qian, T., Dai, A., Trenberth, K. E., and Oleson, K. W.: Simulation of global land surface conditions from 1948 to 2004. Part I: Forcing data and evaluations, J. Hydrometeorol., 7, 953– 975, doi:10.1175/JHM540.1., 2006.

Line 209: Please provide the source of the raw soil moisture image plotted in Figure 1a.

Response:

Thank you for your valuable suggestion. Figure 1a shows the spatial distribution of soil moisture simulated by the CoLM land surface model on May 1, 2016. The aforementioned note has been incorporated into the revised manuscript at Line 260.

Line 266: "The depths of the top three soil layers …" => "The node depths of the top three soil layers …"

Response:

Thank you for your valuable suggestion. We have revised "The depths of the top three soil layers …" to "The node depths of the top three soil layers …".

Line 369: It is not appropriate to refer to soil at the depth of 7-28cm as deep soil.

Response:

Thank you for your valuable suggestion. We have revised “deep soil” to “The soil moisture content at a depth of 7–28 cm.”

Line 445: This is not the reason to develop a new assimilation scheme for land surface model.

Response:

Thank you for your valuable suggestion, and we have revised the sentence to make the reason more clearer.

The original sentences have been changed as follows.

The exchange of heat and water vapor between the land surface and the atmosphere plays a crucial role in influencing weather and climate change. The impact of soil moisture on atmospheric changes is frequently manifested through the persistent influence of large-scale soil moisture anomalies. The construction of an assimilation system with image assimilation capability is aimed at enhancing the spatial structure accuracy of soil moisture anomalies in the initial field of land surface models.

Line 466: Please rephrase this sentence.

Response:

Thank you for your valuable suggestion. The sentence has been revised as follows.

The image assimilation system developed by this study could effectively optimize the spatial structure of soil variables in the background by incorporating constraint conditions of the observed spatial structures. The method demonstrates excellent applicability to various soil variables, effectively

mitigating the negative impact of strong spatial heterogeneity of soil on data assimilation. The key challenge in image assimilation lies in obtaining accurate spatial structure observation of soil variables. The data of ground automatic stations with high spatial-temporal resolution established in China, along with satellite observation data that can overcome natural constraints and achieve large-scale uniform observation in various terrains, are capable of providing observational images depicting the spatial structure of land surface variables for image assimilation. The effective assimilation of the spatial structural characteristics of those high-density meteorological observation data, is the primary focus of our subsequent research. However, how to establish the direct spatial structure relationship between satellite-observed brightness temperature data and soil variables, and how to repair these non-uniform data into uniformly distributed data, these are the key technical problems that need to be solved in the future.

Additionally, it should be noted that the image assimilation method and the prevailing single-point land assimilation method in current practice are not mutually exclusive. The single-point land assimilation method is more suitable for assimilating sparse observation data in key areas. However, if the image assimilation method is used to optimize the fine structure of soil moisture in specific areas, the threshold σ mentioned above needs to be further increased, but this approach is susceptible to introducing additional observational errors. Therefore, by integrating the capacity of the image assimilation method in adjusting the large-scale spatial structure of soil variables and the capability of single-point land assimilation method in finely optimizing soil variables in crucial regions, and by leveraging the advantages offered by diverse types of meteorological observation data, we can attain more refined initial conditions for land models, which constitutes the primary objective of our subsequent research.